High-precision branching-ratio measurement for the superallowed β^+ emitter ^{26}Al^m

P. Finlay,[1,*] G. C. Ball,[2] J. R. Leslie,[3] C. E. Svensson,[1] C. Andreoiu,[4] R. A. E. Austin,[5] D. Bandyopadhyay,[2] D. S. Cross,[4] G. Demand,[1] M. Djongolov,[2] S. Ettenauer,[2,6] P. E. Garrett,[1,2] K. L. Green,[1] G. F. Grinyer,[7] G. Hackman,[2] K. G. Leach,[1] C. J. Pearson,[2] A. A. Phillips,[1] E. T. Rand,[1] C. S. Sumithrarachchi,[1,†] S. Triambak,[1,2,8] and S. J. Williams[2,†]

[1]*Department of Physics, University of Guelph, Guelph, Ontario N1G 2W1, Canada*
[2]*TRIUMF, 4004 Wesbrook Mall, Vancouver, British Columbia V6T 2A3, Canada*
[3]*Department of Physics,Queen's University, Kingston, Ontario K7L 3N6, Canada*
[4]*Department of Chemistry, Simon Fraser University, Burnaby, British Columbia V5A 1S6, Canada*
[5]*Astronomy and Physics Department, Saint Mary's University, Halifax, Nova Scotia B3H 3C3, Canada*
[6]*Department of Physics and Astronomy, University of British Columbia, Vancouver, British Columbia V6T 1Z4, Canada*
[7]*Grand Accélérateur National d'Ions Lourds (GANIL), CEA/DSM-CNRS/IN2P3, Bvd Henri Becquerel, 14076 Caen, France*
[8]*Department of Physics, University of Delhi, Delhi 110 007, India*

(Received 28 March 2012; published 29 May 2012)

A high-precision branching-ratio measurement for the superallowed β^+ emitter ^{26}Al^m was performed at the TRIUMF-ISAC radioactive ion beam facility. An upper limit of $\leqslant$12 ppm at 90% confidence level was found for the second forbidden β^+ decay of ^{26}Al^m to the 2_1^+ state at 1809 keV in ^{26}Mg. An inclusive upper limit of $\leqslant$15 ppm at 90% confidence level was found when considering all possible nonanalog β^+/EC decay branches of ^{26}Al^m, resulting in a superallowed branching ratio of $100.0000^{+0}_{-0.0015}$%.

DOI: 10.1103/PhysRevC.85.055501 PACS number(s): 23.20.Lv, 23.40.−s, 24.80.+y, 27.30.+t

I. INTRODUCTION

Superallowed Fermi β decays provide rigorous tests of the standard electroweak model [1]. These data have validated the conserved vector current (CVC) hypothesis [2] at the level of 1.3×10^{-4} [3], and the vector coupling constant G_V derived from the superallowed data also currently provides the most precise determination of $V_{ud} = G_V/G_F = 0.97425(22)$ [1], the most precisely determined element of the Cabibbo-Kobayashi-Maskawa (CKM) quark mixing matrix. To accurately test the CVC hypothesis and extract a precise value for V_{ud}, the experimental ft values for superallowed Fermi β decays must first be corrected to obtain transition-independent $\mathcal{F}t$ values [1]:

$$\mathcal{F}t \equiv ft(1+\delta_R')(1+\delta_{NS}-\delta_C) = \frac{K}{2\,G_V{}^2\left(1+\Delta_R^V\right)}, \quad (1)$$

where $K/(\hbar c)^6 = 2\pi^3\hbar\ln 2/(m_e c^2)^5 = (8120.278 \pm 0.004) \times 10^{-10}$ GeV^{-4} s, $\Delta_R^V = 2.361 \pm 0.038\%$ [4] is the nucleus-independent component of the radiative correction, δ_R' and δ_{NS} are the nuclear-structure-independent and nuclear-structure-dependent components, respectively, of the radiative correction for each transition, and δ_C accounts for the breaking of isospin symmetry by Coulomb and charge-dependent nuclear forces [5].

Of the thirteen superallowed decays with experimental ft values measured to better than ±0.3%, that of ^{26}Al^m (ft = 3037.53(61) s [6]) is currently the most precise. Additionally, ^{26}Al^m carries the smallest, and most precisely quoted, nuclear-structure-dependent corrections ($\delta_C - \delta_{NS} = 0.305(27)\%$ [5]) of any superallowed emitter, resulting in the most precise corrected $\mathcal{F}t$ value [$\mathcal{F}t$ = 3073.0(12) s] for any superallowed decay by nearly a factor of 2 [6]. The ^{26}Al^m $\mathcal{F}t$ value therefore carries, by far, the largest weight in the current world-average superallowed $\mathcal{F}t$ value ($\overline{\mathcal{F}t}$) used to determine G_V and V_{ud}. An upper limit of <0.007%, established as a byproduct of an ^{26}Al^m Q-value measurement [7], is currently the best experimental upper limit for the total nonsuperallowed β^+/EC decay branches of ^{26}Al^m. While this limit is already smaller than the current uncertainties in the half-life (±0.011%) and f value (±0.017%), it is not entirely negligible. Given the significance of ^{26}Al^m in determining the world-average superallowed $\overline{\mathcal{F}t}$ value, and in anticipation of further high-precision half-life [8] and Q-value measurements for this nucleus that could lead to world-average half-life and f values approaching, or even exceeding, the current experimental upper limit on the nonsuperallowed branching ratio, while performing our recent high-precision half-life measurement for ^{26}Al^m [6] we considered it timely to also establish an improved experimental upper limit on the possible nonsuperallowed decay branches of ^{26}Al^m.

Of the possible nonsuperallowed decay paths open to ^{26}Al^m, the theoretical estimate of the branching ratio for the decay to the $J^\pi = 5^+$ ground state of ^{26}Al^g via an $M5$ transition is 5×10^{-15} for a transition of 1 W.u. including internal conversion. Even a strongly enhanced $M5$ transition would thus yield an entirely negligible branching ratio for the internal decay of ^{26}Al^m. There are, however, four excited states in ^{26}Mg that lie within the Q_{EC} window (Q_{EC} = 4232.66(12) keV [3,9]) of ^{26}Al^m, as illustrated in Fig. 1; the 2_1^+ state at 1809 keV, the 2_2^+ state at 2938 keV, the 0_1^+ state at 3589 keV, and the 3_1^+ state at 3942 keV. The empirical rule that second forbidden nonunique transitions have $\log ft \geqslant 10.6$ [10] suggests β-decay branching ratios to the 2_1^+ and 2_2^+ states, at 1809

*pfinlay314@gmail.com
†Present address: NSCL, Michigan State University, East Lansing, Michigan 48824, USA.

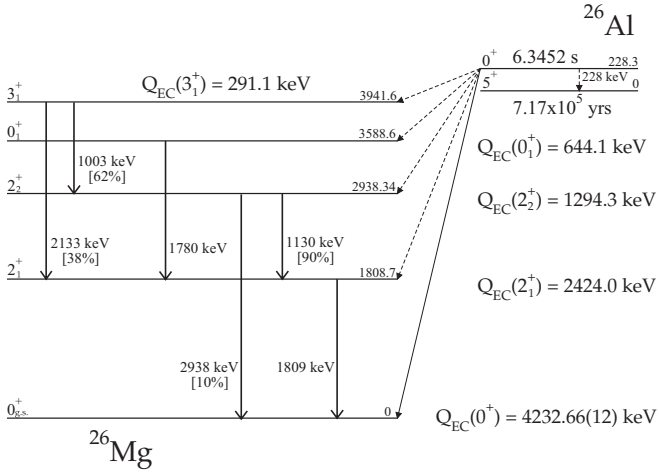

FIG. 1. Low-lying level structure of ^{26}Mg with possible ^{26}Al^m nonanalog decay paths indicated by the dashed arrows. The data are from Refs. [3,6,9,16].

and 2938 keV, below 2×10^{-9} and 1×10^{-11}, respectively. Similarly, following the recommendation of Raman and Gove that second forbidden unique transitions have $\log ft \geqslant 12.8$ [11], the upper limit for the EC transition to the 3_1^+ state at 3942 keV is expected to be a meager 2×10^{-15}, and therefore completely negligible. The electron capture decay to the 0_1^+ state at 3589 keV is, in principle, an "allowed" $0^+ \rightarrow 0^+$ transition and, if it were suppressed only by the ratio of phase-space factors, could have a branching ratio on the order of $f_1/f_0 \approx 2 \times 10^{-5}$. However, as an isospin ladder operator, the Fermi transition operator connects only members of an isospin multiplet and, in the limit of pure isospin symmetry, would concentrate all of the decay strength on the ^{26}Mg ground state (the isobaric analog of ^{26}Al^m), with vanishing matrix elements to the excited 0^+ states of ^{26}Mg. The branching ratio to the 0_1^+ state of ^{26}Mg is thus expected to be suppressed by an additional factor, δ_{C1}^1 [5], that describes the small component of the ^{26}Al^m isobaric analog state mixed into this excited 0_1^+ state due to isospin symmetry breaking. If we assume that all of the strength that is predicted to be removed from the superallowed transition to the ground state due to isospin mixing ($\delta_{C1} = 0.030(10)\%$ [5]) were concentrated in this first excited 0_1^+ state at 3589 keV, the EC decay to this state would have a branching ratio of approximately $(\frac{f_1}{f_0}) \times \delta_{C1} \approx 6(2) \times 10^{-9}$.

There are therefore good theoretical reasons to expect that the *total* nonsuperallowed branching of ^{26}Al^m should not exceed the 10^{-8} level. The largest component of this estimate (the nonanalog Fermi decay to the excited 0_1^+ state) does, however, rely directly on the theoretical calculations of isospin symmetry breaking [5] that one is attempting to constrain by high-precision measurements of superallowed β-decay ft values [12,13]. It thus remains useful to establish a direct experimental upper limit on the total nonsuperallowed branching in ^{26}Al^m decay, which can be adopted without reference to theoretical expectations, and which renders the branching ratio uncertainty negligible in comparison to the uncertainties in the experimental half-life and f-value determinations. Such an improved experimental branching ratio limit for ^{26}Al^m nonsuperallowed decay is presented here.

II. EXPERIMENT

The experiment was performed at TRIUMF's Isotope Separator and Accelerator (ISAC) facility in Vancouver, Canada. A 40-μ A beam of 500-MeV protons bombarded a 14.35 g/cm^2 SiC target, inducing spallation reactions whose products diffused from the heated target. The TRIUMF Resonant Ionization Laser Ion Source (TRILIS) [14] was used to selectively ionize aluminum isotopes, enhancing their abundance relative to the isobaric contaminant ^{26}Na following mass separation of the reaction products. The $A = 26$ beam was delivered as a low-energy (30-keV) beam of 1^+ ions at a rate of approximately 10^6 ^{26}Al^m/s ($T_{\frac{1}{2}} = 6.34654(76)$ s [6]), 10^7 ^{26}Na/s ($T_{\frac{1}{2}} = 1.07128(25)$ s [15]), and 10^9 ^{26}Al^g/s ($T_{\frac{1}{2}} = 7.17(24) \times 10^5$ yr [16]) onto a 13-mm-wide, 50-μ m-thick, and 120-m-long continuous loop of Mylar-backed iron-oxide tape located at the mutual centers of the 8π spectrometer [17], an array of 20 Compton-suppressed HPGe detectors, and SCEPTAR [18,19], an array of 20 1.6-mm-thick plastic scintillators. SCEPTAR was used to tag the $\beta^{\pm}$ particles emitted following the decay of the sample, while the 8π spectrometer was used to detect the emitted γ rays. To reduce the sensitivity to the very long lived ^{26}Al^g, the portion of the tape containing the previous sample was moved out of the array to a collection box, located approximately 1.5 m behind the array and shielded by a 5.1-cm-thick lead wall, prior to the start of a new counting cycle.

The measurement cycles were characterized by a 2-s tape move followed by 4 s of background counting before the beam was implanted on the tape for 21 s so as to saturate the activity of ^{26}Al^m ($T_{\frac{1}{2}} = 6.34654$ s [6]). The beam was then deflected at the ion source (two floors below the experimental hall) by an electrostatic kicker, and the sample at the center of the arrays was allowed to decay for 47 s before the tape was moved and the process was repeated. The β activity from a typical cycle, recorded in a multichannel scalar (MCS) that was active throughout the entire cycle, is depicted in Fig. 2. A total of 2188 such cycles were registered over the course of the experiment. Of these, 54 (2.5%) were rejected due to a loss of protons on the primary production target during the implantation phase of the cycle.

Full list-mode event data, including energies and times relative to the start of the cycle, were recorded during the first 6.4 s and the last 44 s of each cycle, but these were vetoed between cycle times of 6.4 and 30 s when the activity was dominated by the short-lived ^{26}Na ($T_{\frac{1}{2}} = 1.07128$ s [15]) contaminant. For the list-mode data, triggers were generated by γ singles, $\gamma\gamma$ coincidences, $\beta\gamma$ coincidences, and scaled-down β singles (with a scale down factor of 100) events. The individual detector times were recorded relative to the master trigger in TDCs with 0.5-ns precision, and in addition the trigger times for all β and γ events were recorded relative to the start of the cycle using separate LeCroy 2367 universal logic modules (ULMs) scaling a 10 MHz $\pm$ 0.1 Hz Stanford

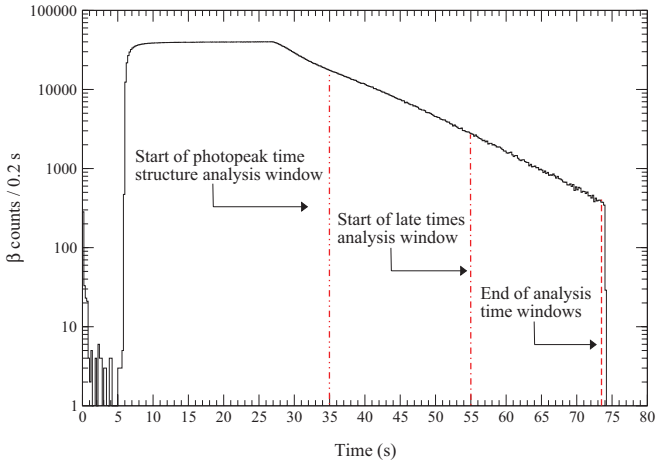

FIG. 2. (Color online) Total recorded β activity for a typical cycle. The beam, comprised of $\sim 10^6$/s ^{26}Al^m ($T_{\frac{1}{2}} = 6.34654(76)$ s [6]), $\sim 10^7$/s ^{26}Na ($T_{\frac{1}{2}} = 1.07128(25)$ s [15]), and $\sim 10^9$/s ^{26}Al^g ($T_{\frac{1}{2}} = 7.17(24)\times 10^5$ yr [16]), is turned on at $t = 6$ s following a 2-s tape move and 4 s of background counting. The beam is on for 21 s, and then allowed to decay for 47 s before the cycle is repeated. These data are from an MCS unit that recorded β events from SCEPTAR throughout the cycle, while the list mode event data used in the detailed analysis were vetoed between cycle times of 6.4 and 30 s when the activity was dominated by the short-lived ^{26}Na contamination. Two analysis windows for ^{26}Al^m decay are shown from cycle times of 35.1 to 73.5 s (starting 8.1 s after beam off) when analyzing the time structure of the 1809-keV photopeak and a "late times" analysis window from cycle times of 55 to 73.5 s, starting 28 s after beam was turned off when the ^{26}Na contaminant activity had decayed to a negligible level.

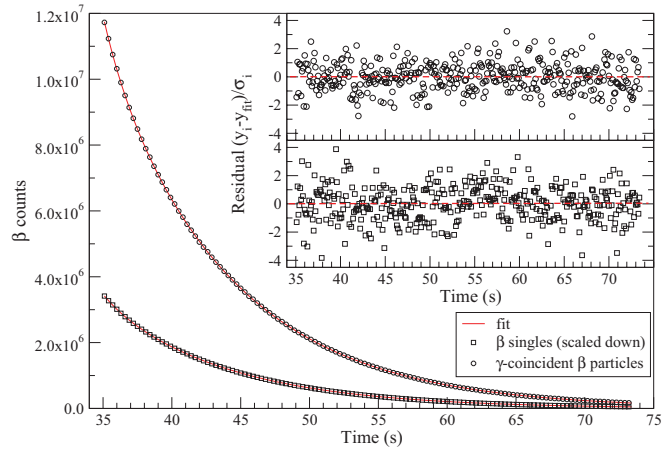

FIG. 3. (Color online) Fit to the singles (scaled down by 100) and γ-coincident β activities, summed for all 2134 good cycles. For clarity, the error bars have been suppressed and only every third data point is displayed in the β activity curves.

Research Systems SRS-SC10 precision oscillator, giving an event time stamp with 100-ns precision.

III. ANALYSIS OF THE SCEPTAR β DATA

During the offline analysis of the SCEPTAR data, 2 of the 20 scintillator paddles were found to have malfunctioned during the measurement, and so data from these 2 detectors were not used in the analysis. To determine the total number of ^{26}Al^m β^+ particles detected in the remaining 18 detectors, the scaled-down β-singles and γ-coincident β activity curves from the ULM data were dead-time corrected and summed over all good cycles (Fig. 3). Both curves were fit using a maximum-likelihood routine [15,20] based on a Levenberg-Marquardt algorithm. The fit function included components of ^{26}Na, ^{26}Al^m, and a constant component which accounted for both background and the decay of the very long lived ^{26}Al^g. The half-lives of ^{26}Al^m ($T_{\frac{1}{2}} = 6.34654(76)$ s [6]) and ^{26}Na ($T_{\frac{1}{2}} = 1.07128(25)$ s [15]) were fixed to their previously measured values, while the activities of both species, as well as the constant background activity, were free parameters. The resulting fit to the SCEPTAR β data is shown in Fig. 3 and yielded a total of $2.944(29)\times 10^9$ ^{26}Al^m β^+ particles detected between cycle times of 35.1 and 73.5 s and $3.024(42) \times 10^8$ ^{26}Al^m β^+ particles detected during the "late time" analysis window between cycle times of 55 and 73.5 s, once corrected for the scale-down factor of 100 applied to the β-singles data.

When utilizing β-coincident γ-ray data to determine branching ratios for particular transitions, it is not necessary to determine the absolute efficiency of SCEPTAR, as this efficiency affects both the detected number of β-coincident γ rays and the detected number of β particles, and it cancels in the ratio. The $\beta\gamma$-coincidence data from this measurement, however, will not include any potential contribution to the total nonanalog decay strength of ^{26}Al^m arising from electron captures, including to the 0_1^+ state at 3.6 MeV, which lies outside the Q_{β^+} window of ^{26}Al^m. The SCEPTAR efficiency must therefore be determined to establish limits on the branching ratios for such EC decay branches using the γ-ray singles data.

The SCEPTAR efficiency was determined by taking the ratio of the β-coincident 1809-keV γ-ray photopeak area to the 1809-keV peak area in γ singles run by run. As the 1809-keV γ ray in this experiment arises almost entirely from the β^- decay of ^{26}Na, a GEANT4 [21] Monte Carlo simulation, including detailed representations of both the 8π spectrometer and SCEPTAR, was performed to compare the efficiency of SCEPTAR for β^+ transitions from ^{26}Al^m to the β^- decay of ^{26}Na for the three possible β^+ decay branches of ^{26}Al^m. The results from the Monte Carlo simulation are shown in Fig. 4, and they verify that for the superallowed β^+ transitions from ^{26}Al^m to the ground state of ^{26}Mg (effectively 100% of ^{26}Al^m decays) the SCEPTAR efficiency is the same as for the ^{26}Na β^- decays feeding the 1809-keV level to within $\pm 2\%$ for all deposited energy thresholds below 300 keV. We thus adopt a ratio of 1.00(2) between the ^{26}Na and ^{26}Al^m β efficiencies to obtain an efficiency for ^{26}Al^m β^+ decays of $76.8\% \pm 1.6\%$, yielding a total of $3.83(9)\times 10^9$ ^{26}Al^m β^+ particles emitted between 35.1 and 73.5 s in the decay portion of the cycle and $3.94(10)\times 10^8$ emitted during the "late time" window from 55 to 73.5 s.

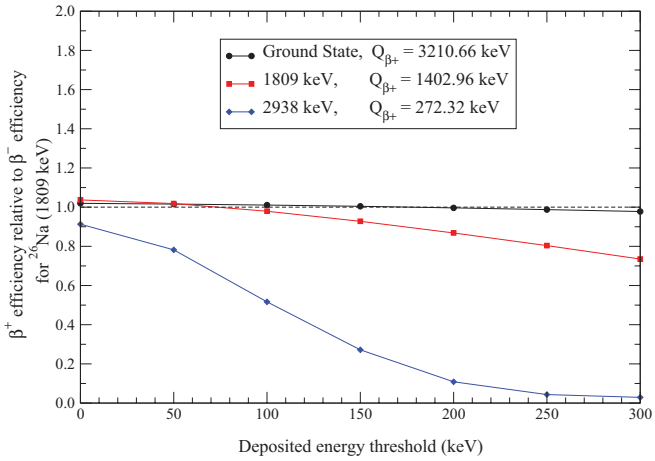

FIG. 4. (Color online) GEANT4 simulation of the number of detected counts vs SCEPTAR deposited-energy threshold for each of the possible β^+ branches in ^{26}Al^m, normalized to the number of counts detected for ^{26}Na β^- decay. The deposited energy threshold in the current experiment was between 50 and 100 keV. These simulations verify that the β^+ detection efficiency for ^{26}Al^m decays to the ground state of ^{26}Mg is the same as for ^{26}Na β^- decays to within ∼2% for all deposited-energy thresholds below 300 keV.

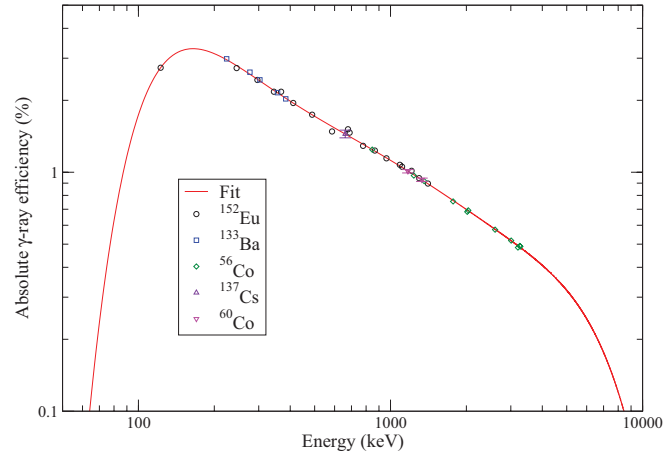

FIG. 5. (Color online) Absolute γ-ray photopeak efficiency curve for the 8π spectrometer. The absolute efficiency at 1809 keV was determined to be 0.750(15)%.

IV. ANALYSIS OF THE 8π γ-RAY DATA

Gamma-ray photopeak efficiency data were collected immediately following the ^{26}Al^m branching ratio measurement. Decays from sealed sources of ^{133} Ba, ^{152} Eu, and ^{56} Co placed sequentially at the center of the array were measured over a period of several hours to provide a relative efficiency calibration from $E_\gamma \sim 0.1$ MeV to $E_\gamma \sim 3.2$ MeV. The fit function $\ln(\epsilon) = \sum_{i=0}^{8} a_i (\ln E)^i$, where ϵ is the efficiency of the 8π array at γ-ray energy E (in MeV), was used to fit the relative efficiency curve [22]. Calibrated γ-ray sources of ^{60} Co (±1.9% and ±3.1%) and ^{137} Cs (±3.7%) were used to provide an absolute normalization to the relative efficiency curve, resulting in the absolute γ-ray detection efficiency curve shown in Fig. 5. The absolute efficiency for the 1809-keV γ ray was determined to be 0.750(15)%.

A. The β-coincident γ-ray data

As can be seen from Fig. 1, only the 2_1^+ and 2_2^+ levels in ^{26}Mg, at 1809 and 2938 keV, respectively, have positive Q_{β^+} values. Since the 2_2^+ level at 2938 keV γ decays with a 90% branch to the 2_1^+ level at 1809 keV, the 2_1^+ level (in principle) acts as a collector state for both possible nonsuperallowed β^+ decay branches of ^{26}Al^m. As shown in Fig. 4, the β^+ detection efficiency is significantly lower for the low $Q_{\beta^+} = 272$ keV decay to the 2_2^+ state. Furthermore, the phase-space integral for the 2_2^+ state is more than two orders of magnitude smaller than for the 2_1^+ state, and any decay to the 2_2^+ state with $Q_{EC} = 1294$ keV and $Q_{\beta^+} = 272$ keV would be expected to be mostly by electron capture. A limit on the detection of 1809-keV γ rays in coincidence with β^+ particles from ^{26}Al^m decay is thus primarily a limit on the β^+ decay branch to the 2_1^+ state at 1809 keV. Three separate analyses of the β-coincident γ-ray data were performed to establish this upper limit on the second forbidden β^+ decay of ^{26}Al^m to the 2_1^+ state in ^{26}Mg at 1809 keV.

1. β-coincident 1809-keV γ-ray peak area at late times

The approach of using the 1809-keV γ-ray to quantify the nonsuperallowed decay strength of ^{26}Al^m is complicated by the large contaminants of ^{26}Na and ^{26}Al^g present in the beam, since more than 88% of ^{26}Na decays, and approximately 100% of ^{26}Al^g decays, proceed through the 2_1^+ level in ^{26}Mg at 1809 keV and thus also emit the 1809-keV γ-ray of interest. Fortunately, the half-lives for ^{26}Na, ^{26}Al^m, and ^{26}Al^g, ∼1 s, ∼6 s, and ∼700 000 yr, respectively, differ significantly and can be exploited to identify each isotope's contribution to the 1809-keV γ-ray photopeak.

A matrix of β-coincident γ-ray energies versus time relative to the start of the cycle was generated cycle by cycle and summed over all good cycles. A gate was placed on cycle times between 55 and 73.5 s, 28 s (26 ^{26}Na half-lives) after beam-off, and the γ-ray energy spectrum associated with these late times was projected. The resulting γ-ray energy spectrum around 1809 keV appears in Fig. 6(a). The expected location of the 1809-keV photopeak was fit using the germanium-peak-fitting program GF3 included as part of the RADWARE software package [23]. The peak-shape parameters and centroid were constrained to the values determined from the fit to the 1809-keV peak from the full projection of the matrix, with only the background level and slope, and with the peak area left free when fitting the time-gated spectrum in Fig. 6(a). Based on the beam rates of ^{26}Na and ^{26}Al^g, they are expected to contribute 0.7 and 1.0 counts to the 1809-keV photopeak over this time region, respectively. Subtracting these counts from the fitted peak area yields −2(13) counts in the 1809-keV photopeak attributable to ^{26}Al^m decays. Correcting for γ-ray efficiency and dividing by the total number of ^{26}Al^m β^+ decays detected

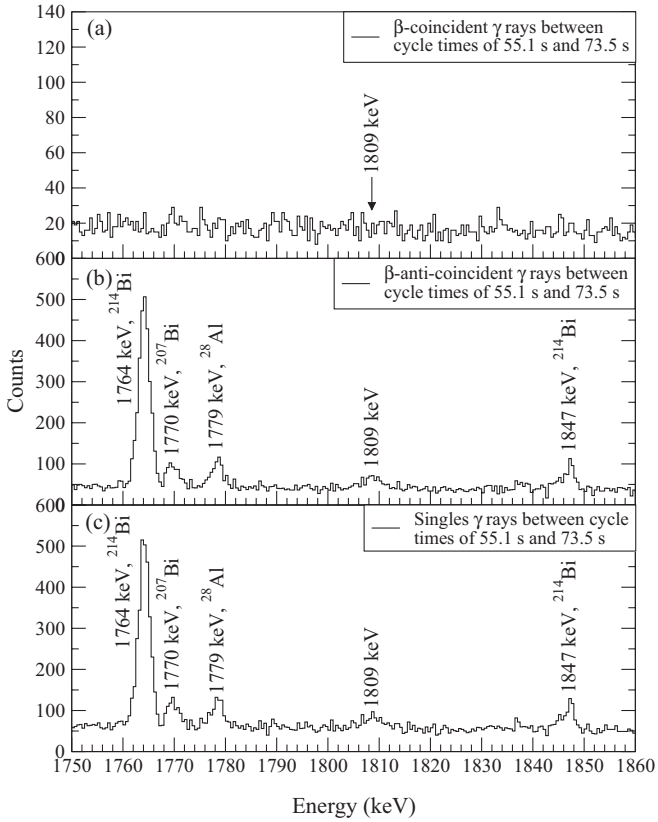

FIG. 6. Portion of γ-ray energy spectra for cycle times between 55 and 73.5 s for (a) β-coincident γ rays, (b) β-anticoincident γ rays, and (c) all γ rays.

over this portion of the cycle [$3.024(42) \times 10^8$ β^+ decays] yields a branching ratio to the 2_1^+ level of -0.9 ± 5.7 ppm.

2. *Time structure of the β-coincident 1809-keV γ rays*

For the same matrix of γ-ray energy versus cycle time described in Sec. IV A1, a 16-channel-wide energy gate (0.5 keV/channel) was placed about the 1809-keV photopeak. The activity curve derived from the times associated with the γ-ray events within this gate was dead-time and pile-up corrected [24], then fit using the same function as was used to fit the β activity described in Sec. III. The energy gate and dead-time- and pile-up-corrected activity curve and fit components for the 1809-keV photopeak appear in Fig. 7. Correcting for the γ-ray efficiency at 1809 keV [0.750(15)%] yields a total of $3.41(20)\times10^5$ photons in the 1809-keV gate associated with the ^{26}Al^m half-life. While it appears that there is a large ^{26}Al^m component to the activity curve for the 1809-keV γ ray, one must account for the background underneath the photopeak due to bremsstrahlung photons arising from the β^+ particles emitted in the superallowed decay of ^{26}Al^m, which will have the same time structure as any real 1809-keV γ rays emitted following nonanalog decay of ^{26}Al^m. To quantify the bremsstrahlung contribution to the 1809-keV-gated activity curve, a second energy gate 112 channels wide was placed around the background region immediately above the 1809-keV photopeak. The energy gate,

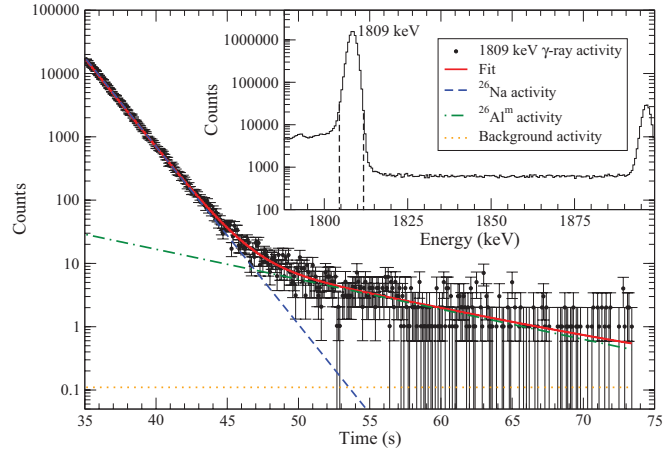

FIG. 7. (Color online) Activity curve, with fit components overlaid, for the 16-channel-wide energy gate (inlaid) on the 1809-keV photopeak derived from the β-coincident γ-ray data. The number of events in this gate associated with the half-life of ^{26}Al^m is 2561(140), during the analysis time window from 35.1 to 73.5 s.

dead-time-corrected activity curve, and fit components for the background region above the 1809-keV photopeak appear in Fig. 8. Scaling to the number of channels used in the photopeak gate, and correcting for the difference in the yield of, and detector response to, the ^{26}Al^m bremsstrahlung spectrum over the two regions (95% $\pm$ 5%) as determined from the GEANT4 simulation described in Sec. III, yields $3.44(16)\times10^5$ ^{26}Al^m bremsstrahlung photons in the 1809-keV gate. Subtracting these from the photopeak gate, and dividing by the total number of detected ^{26}Al^m β^+ particles from Sec. III, yields a branching ratio to the 2_1^+ level of -1.0 ± 10.0 ppm.

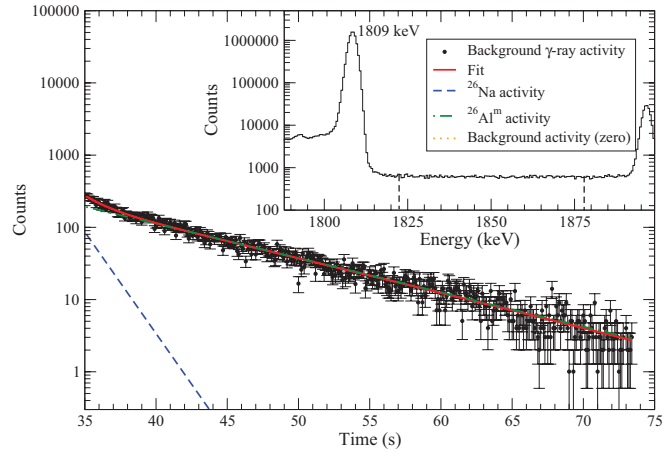

FIG. 8. (Color online) Activity curve, with fit components overlaid, for the 112-channel-wide energy gate (inlaid) on the background region above the 1809-keV photopeak derived from the β-coincident γ-ray data. The number of events in this gate associated with the half-life of ^{26}Al^m is 17163(202), during the analysis time window from 35.1 to 73.5 s.

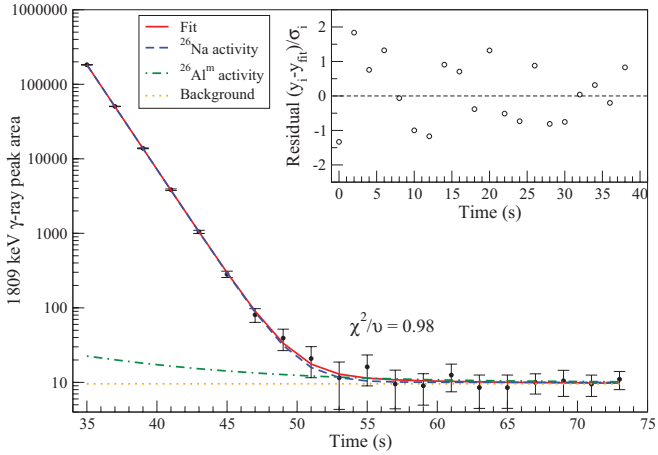

FIG. 9. (Color online) The pile-up- and dead-time-corrected β-coincident 1809-keV γ-ray peak area, measured over successive 2-s time bins, plotted vs time over the decay portion of the cycle. The total number of counts attributed to ^{26}Al^{m} from the fit is 112(121) during the analysis time window from 35.1 to 73.5 s. A constant offset of 10 has been added to the data plotted here for clarity.

3. *β-coincident 1809-keV γ-ray peak area versus time*

For the same matrix of γ-ray energies versus times described in Sec. IV A1, successive 2-s time gates were placed on the γ-ray activity curve, and the associated γ-ray energy spectra were projected. The 1809-keV photopeak in each 2-s gate was then fit with the peak-shape parameters constrained as discussed in Sec. IV A1, generating the 1809-keV photopeak area versus time curve that appears in Fig. 9. This curve was dead-time and pile-up corrected, then fit using the same fitting routine as described in Sec. III. The advantage of this method over that described in Sec. IV A2 is that by fitting the 1809-keV γ-ray peak areas, the bremsstrahlung due to the ^{26}Al^{m} β^+ decays, which will have the same time structure as 1809-keV γ rays emitted following nonsuperallowed decay of ^{26}Al^{m}, is removed by considering only the 1809-keV peak area above background.

The total number of 1809-keV γ rays attributed to ^{26}Al^{m} from the fit to the peak area versus time curve in Fig. 9 is 112(121). Correcting for efficiency and dividing by the total number of detected ^{26}Al^{m} β^+ particles from Sec. III yields a branching ratio to the 2_1^+ level of 5.1 ± 5.5 ppm.

B. The β-anticoincident γ-ray data ($\overline{\beta}$-γ)

The potential nonsuperallowed decay branches of ^{26}Al^{m} that would proceed by electron capture (to the 0_1^+, 3_1^+, and 2_2^+ states), or the internal $M5$ γ decay, would not be in coincidence with β particles, and they are thus individually searched for most sensitively in the $\overline{\beta}$-γ spectrum.

For completeness, experimental limits were placed on all possible decay paths open to ^{26}Al^{m} by fitting the expected locations of γ rays that would be emitted following ^{26}Al^{m} nonsuperallowed decay. In each case the peak shape parameters and centroid were constrained to the values determined from the fits to the large number of γ rays from ^{26}Na decay [15] in

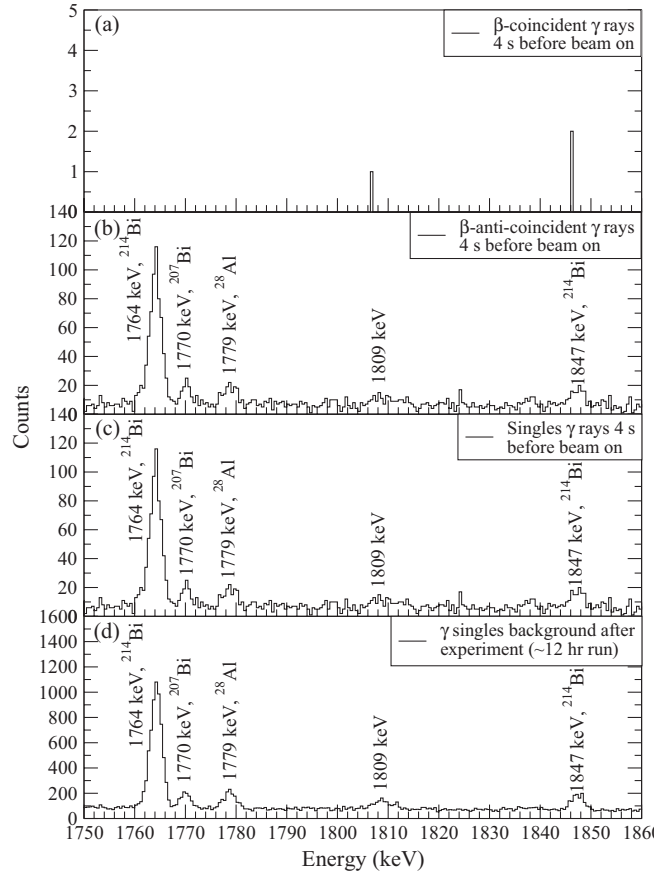

FIG. 10. Portion of (a) β-coincident, (b) β-anticoincident, and (c) singles γ-ray energy spectra for the 4 s before beam on, summed over all 2134 good cycles, and (d) a γ-ray singles spectrum recorded for the ∼12 h immediately following the experiment while the primary proton beam was incident on the production target, but no beam was being implanted in the array. The relative intensities of the γ rays in spectra (b) through (d) are consistent and verify that they do not arise from short-lived components of the radioactive beam.

the full projection of the matrix, with only the background shape and peak area left free when fitting the time-gated γ-ray spectra. This analysis is complicated for the 1780-keV transition that would arise from EC decay to the 0_1^+ state of ^{26}Mg, due to the presence of a background γ ray at 1779 keV [see Fig. 10(d)] arising from the decay of ^{28}Al ($T_{1/2}$ = 2.2414 min [16]) produced in ^{27}Al (n, γ) capture reactions by neutrons emitted from the primary production target. To determine the contribution to the 1780-keV photopeak from this background, a gate was placed on the 4 s before the beam was implanted onto the tape, during the "background counting" portion of the cycle. The resulting γ-ray energy spectrum appears in Fig. 10(b). The 1780-keV peak was fit subject to the same constraints described above, yielding a peak area of 81(14), which was then scaled to the same number of time channels as the gate between 55 and 73.5 s, and subtracted from the measured peak area in Fig. 6(b). Table I lists peak areas for the γ-ray transitions listed in Fig. 1,

TABLE I. Upper limits for the individual γ-ray transitions that could be emitted following nonsuperallowed decays of $^{26}Al^m$, derived from the $\overline{\beta}$-γ data. The peak areas are for cycle times between 55 and 73.5 s and have been efficiency corrected. The deduced upper limit on the branching ratio to each level at 90% confidence level (CL) is based on the renormalized probability density function for positive peak areas as discussed in the text. For each of those levels with more than one γ-ray transition, the renormalized PDFs have been combined according to the γ-ray branching ratios (BRs) to give a single upper limit on the branching ratio to that level.

Level (J^π, E)	γ ray (keV)	Peak area (ppm)	γ-ray branching ratio (%)	Upper limit on BR to level (90% CL in ppm)
3_1^+, 3942 keV	1003	11(12)	62	16
	2133	−10(6)	38	
0_1^+, 3589 keV	1780	−12(25)	100	34
2_2^+, 2938 keV	1130	3(10)	90	21
	2938	4(6)	10	
5^+, $^{26}Al^g$	228	3(15)	100	27

as well as upper limits on the individual level branching ratios at the 90% confidence level.

C. The γ-ray singles data

While the 1809-keV γ ray in the β-γ coincidence data sets a limit on the β^+ decay to the 2_1^+ state, and analysis of the $\overline{\beta}$-γ data listed above places experimental limits on the individual EC decay branches and $M5$ internal γ decay, a more sensitive limit on the total nonsuperallowed β^+/EC decay of $^{26}Al^m$ can be obtained by noting that decay of the 2_2^+, 3_1^+, and 0_1^+ states feed the 2_1^+ 1809-keV level with 90%, 94%, and 100% probabilities, respectively. The 1809-keV level thus acts as an effective collector of all nonsuperallowed β^+/EC decays of $^{26}Al^m$, and measurement of the 1809-keV γ ray without any conditions on whether or not a β particle is detected in coincidence (i.e. the γ-ray singles data) thus provides a limit on the total nonsuperallowed β^+/EC decay of $^{26}Al^m$.

1. 1809-keV γ-ray-peak area at late times

A matrix of all γ-ray energies versus time relative to the start of the cycle was generated cycle by cycle and summed over all good cycles. A gate was placed on cycle times between 55 and 73.5 s, and the γ-ray energy spectrum associated with these late times was projected. The resulting γ-ray energy spectrum around 1809 keV appears in Fig. 6(c). The 1809-keV photopeak was fit following the same procedure outlined in Sec. IV A1. Based on the beam rate of ^{26}Na and $^{26}Al^g$, they are expected to contribute 0.9 and 1.2 counts to the 1809-keV photopeak over this time region, respectively. Subtracting these counts from the fitted peak area yields 168(29) counts remaining in the 1809-keV photopeak. This analysis is also complicated by the presence of a background γ ray at 1809 keV [see Figure 10(d)], which is only observed when the primary proton beam is on and is believed to arise from neutrons emitted from the primary production target populating the first excited state of ^{26}Mg in surrounding materials through reactions such as ^{25}Mg(n,γ), ^{26}Mg$(n,n'\gamma)$, and/or ^{29}Si(n,α). To determine the number of background decays contributing to the 1809-keV photopeak in Fig. 6(c), a gate was placed on the 4 s of background counting before the beam was implanted onto the tape. The resulting γ-ray energy spectrum summed over all 2134 good cycles appears in Fig. 10(c). The 1809-keV γ ray from this spectrum was fit with the same constraints described above, yielding a total of 38(10) counts in the photopeak arising from background radiation. Scaling to the same number of time channels used in the decay gate yields 184(48) counts, which, when subtracted from the peak area measured between cycle times of 55 and 73.5 s, leaves −16(56) counts attributed to $^{26}Al^m$ decay. Correcting for γ-ray efficiency and dividing by the total number of $^{26}Al^m$ β^+ decays emitted over this portion of the cycle [$3.94(10)\times10^8$ β^+ decays] yields a total nonsuperallowed β^+/EC decay branching ratio for $^{26}Al^m$ of -5 ± 19 ppm.

2. Time structure of the 1809-keV γ rays

For the same matrix of γ-ray energy versus time described in Sec. IV C1, a 16-channel-wide energy gate (0.5 keV/channel) was placed about the 1809-keV photopeak. The activity curve derived from the times associated with the γ-ray events within this gate was dead-time and pile-up corrected, then fit using the same function as described in Sec. III. The energy gate, dead-time- and pile-up-corrected activity curve, and fit components for the 1809-keV photopeak appear in Fig. 11. Correcting for the γ-ray efficiency yields a total of $5.1(3)\times10^5$ photons in the 1809-keV gate associated with the half-life of $^{26}Al^m$. A second energy gate 112 channels wide was placed on the background region immediately above the 1809-keV photopeak to quantify the bremsstrahlung contribution to the 1809-keV gated activity curve. The energy gate, dead-time-corrected activity curve, and fit components for the background region above the 1809-keV photopeak appear in Fig. 12. Scaling to the number of channels used in the photopeak gate, and correcting for both the energy dependence of the bremsstrahlung spectrum between the two regions as well as the detector response to the bremsstrahlung over this energy region ($94\% \pm 4\%$), yields $5.15(59)\times10^5$ $^{26}Al^m$ bremsstrahlung photons in the 1809-keV gate. Subtracting

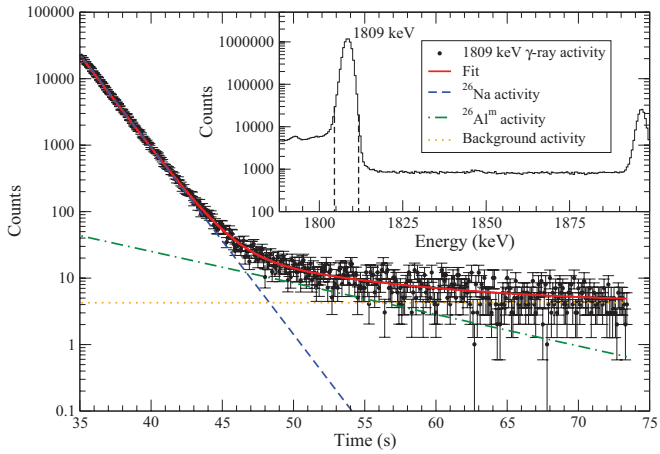

FIG. 11. (Color online) Activity curve, with fit components overlaid, for the 16-channel-wide energy gate (inlaid) on the 1809-keV photopeak derived from the γ-ray singles data. The number of γ rays in this gate associated with the half-life of ^{26}Al^{m} is 3858(217), during the analysis time window from 35.1 to 73.5 s.

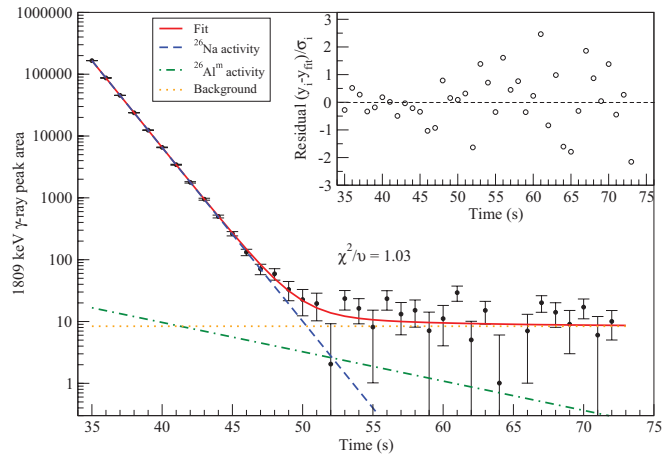

FIG. 13. (Color online) The pile-up- and dead-time-corrected 1809-keV γ-ray singles peak area, measured over successive 1-s time bins, plotted vs time over the decay portion of the cycle. The total number of counts attributed to ^{26}Al^{m} from the fit is 158(185) during the analysis time window from 35.1 to 73.5 s.

these from the photopeak gate, and dividing by the total number of emitted ^{26}Al^{m} β^+ particles from Sec. III, yields a total nonsuperallowed β^+/EC branching ratio for ^{26}Al^{m} of 0 ± 17 ppm.

3. 1809-keV γ-ray peak area versus time

Successive 1-s time gates were placed on the γ-ray activity curve, and the associated γ-ray energy spectra were projected from the matrix described in Sec. IV C1. The 1809-keV photopeak in each 1-s gate was then fit with the peak-shape parameters constrained as discussed in Sec. IV A1, generating the 1809-keV photopeak area versus time curve that appears in Fig. 13. This curve was dead-time and pile-up corrected,

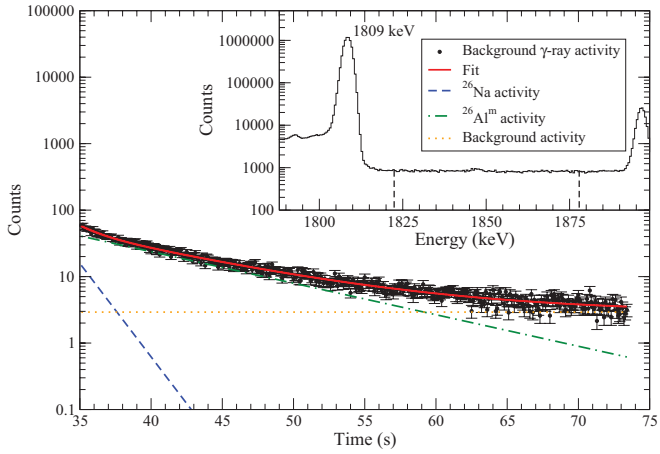

FIG. 12. (Color online) Activity curve, with fit components overlaid, for the 112-channel-wide energy gate (inlaid) on the background region above the 1809-keV photopeak derived from the γ-ray singles data. The number of γ rays in this gate associated with the half-life of ^{26}Al^{m} is 25405(292), during the analysis time window from 35.1 to 73.5 s.

then fit using the same fitting routine as described in Sec. III. The activity of the 1809-keV peak area does not go to zero at late times due to the presence of the background radiation at 1809 keV in the γ-singles spectrum [see Fig. 10(d)]. This activity is, however, constant in time and is thus accounted for by the background parameter in the fit function. The rate for the constant activity component of the fit was determined to be $3.7(9) \times 10^{-3}$/s, consistent with the value of $4.7(14) \times 10^{-3}$/s from the 1809-keV peak area in the 4-s background counting region of the cycle prior to beam on shown in Fig. 10(c).

The total number of 1809-keV γ rays attributed to ^{26}Al^{m} from the fit to the peak area versus time data is 158(186). Correcting for γ-ray efficiency and dividing by the total number of emitted ^{26}Al^{m} β^+ particles from Sec. III yields a total nonsuperallowed β^+/EC branching ratio for ^{26}Al^{m} of 5.5 ± 6.5 ppm.

V. RESULTS

The total nonsuperallowed β^+/EC branching ratios calculated in Secs. IV C1, IV C2, and IV C3, -5 ± 19, 0 ± 17, and 5.5 ± 6.5 ppm, respectively, are all consistent with zero. These values are also in agreement with the upper limit for the nonsuperallowed decay of ^{26}Al^{m} of 7×10^{-5} reported in Ref. [7], but they provide a lower (1σ) upper limit by nearly an order of magnitude.

Of the three limits presented above, the most precise is that obtained from the measured 1809-keV peak area versus time. However, the value 5.5 ± 6.5 ppm allows for a negative total nonsuperallowed β^+/EC ^{26}Al^{m} branching ratio, which is unphysical. The Gaussian probability distribution function (PDF) with mean $\mu = 5.5$ and $\sigma = 6.5$, as well as that with the same μ and σ but renormalized to give unit probability integrated over only positive values, is shown in Fig. 14(a). The renormalized PDF, which no longer contains unphysical values, gives upper limits for the total nonsuperallowed β^+/EC

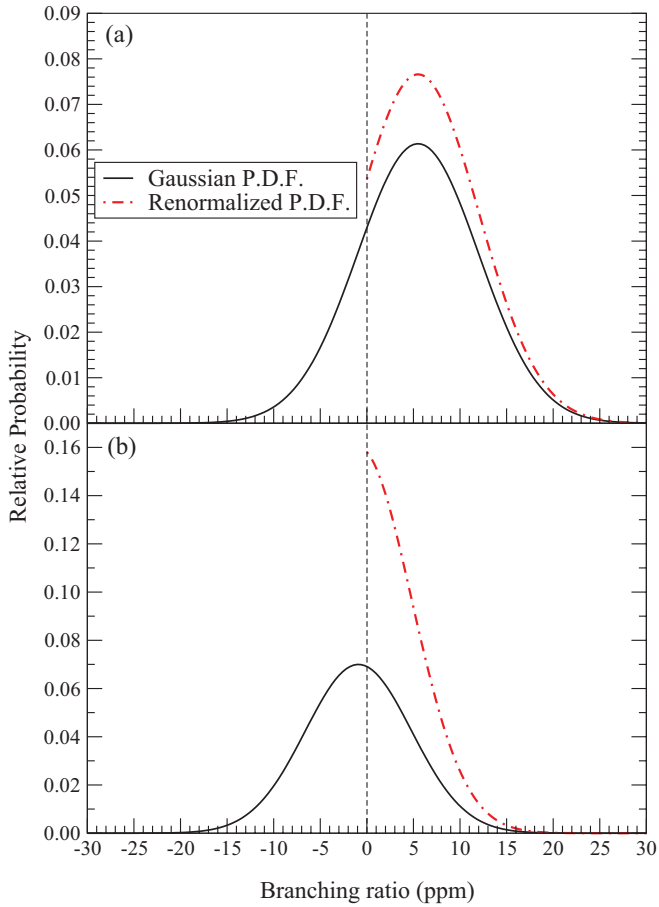

FIG. 14. (Color online) The Gaussian PDF and the renormalized PDF for (a) the total nonsuperallowed branching ratio of ^{26}Al^m calculated in Sec. IV C3 and (b) the ^{26}Al^m β^+ branching ratio to the 2_1^+ state at 1809 keV calculated in Sec. IV A1. The renormalized PDFs yield upper limits of (a) 10 and 15 ppm at 67% and 90% CL, respectively, and (b) 5 and 12 ppm at 67% and 90% CL, respectively.

^{26}Al^m branching ratio of 10 ppm at 67% (1σ) confidence level (CL), and 15 ppm at 90% (3σ) CL.

Of all the individual nonsuperallowed decay branches open to ^{26}Al^m, only β^+ decay to the 2_1^+ level at 1809 keV could be experimentally constrained more tightly than the inclusive nonsuperallowed β^+/EC branching ratio. The branching ratios, calculated in Secs. IV A1, IV A2, and IV A3 to be -0.9 ± 5.7, -1.0 ± 10.0, and 5.1 ± 5.5 ppm, respectively, are also all consistent with zero. In this case, where a β-γ coincidence analysis could be used, the "late time" window analysis of Sec. IV A1 provided the most precise limit. The Gaussian PDF for the branching ratio from Sec. IV A1, along with the renormalized PDF, is shown in Fig. 14(b). The renormalized PDF gives upper limits for the second forbidden ^{26}Al^m β^+ branching ratio to the 2_1^+ state at 1809 keV of 5 ppm at 67% CL and 12 ppm at 90% CL.

For completeness, we also determined experimental upper limits for the other individual decay branches although, as noted above, they are less stringent than the limit on the total nonsuperallowed β^+/EC decay of ^{26}Al^m. These are 16, 34, 21, and 27 ppm at 90% CL for nonsuperallowed decay to the 3_1^+, 0_1^+, and 2_2^+ states and for the internal $M5$ transition, respectively.

VI. CONCLUSIONS

A search for nonsuperallowed decay branches of the nucleus ^{26}Al^m has established an upper limit of 10 ppm at 67% CL and 15 ppm at 90% CL, for the total nonsuperallowed β^+/EC decay of ^{26}Al^m. A tighter limit of 5 ppm at 67% CL and 12 ppm at 90% CL has also been established for the second forbidden β^+ decay of ^{26}Al^m to the 2_1^+ state at 1809 keV in ^{26}Mg. As the $M5$ internal γ decay of ^{26}Al^m can safely be assumed to be negligible, we adopt the new experimental upper limit on the total nonsuperallowed β^+/EC decay of 15 ppm at 90% CL to establish a precise experimental branching ratio for ^{26}Al^m of $100.0000 \pm^{0}_{0.0015}$ %.

ACKNOWLEDGMENTS

This work has been partially supported by the Natural Sciences and Engineering Research Council of Canada. TRIUMF receives federal funding via a contribution agreement with the National Research Council of Canada.

[1] I. S. Towner and J. C. Hardy, Rep. Prog. Phys. **73**, 046301 (2010).
[2] R. P. Feynman and M. Gell-Mann, Phys. Rev. **109**, 193 (1958).
[3] J. C. Hardy and I. S. Towner, Phys. Rev. C **79**, 055502 (2009).
[4] W. J. Marciano and A. Sirlin, Phys. Rev. Lett. **96**, 032002 (2006).
[5] I. S. Towner and J. C. Hardy, Phys. Rev. C **77**, 025501 (2008).
[6] P. Finlay *et al.*, Phys. Rev. Lett. **106**, 032501 (2011).
[7] S. W. Kikstra *et al.*, Nucl. Phys. A **529**, 39 (1991).
[8] J. C. Hardy (private communication).
[9] T. Eronen *et al.*, Phys. Rev. Lett. **97**, 232501 (2006).
[10] B. Singh, J. L. Rodriguez, S. S. M. Wong, and J. K. Toli, Nucl. Data Sheets **84**, 487 (1998).
[11] S. Raman and N. B. Gove, Phys. Rev. C **7**, 1995 (1973).
[12] G. F. Grinyer, C. E. Svensson, and B. A. Brown, Nucl. Instrum. Methods Phys. Res., Sect. A **622**, 236 (2010).
[13] I. S. Towner and J. C. Hardy, Phys. Rev. C **82**, 065501 (2010).
[14] C. Geppart *et al.*, Nucl. Phys. A **746**, 631c (2004).
[15] G. F. Grinyer *et al.*, Phys. Rev. C **71**, 044309 (2005).
[16] Richard B. Firestone, *Table of Isotopes*, 8th ed. (Wiley-Interscience, New York, 1996).
[17] C. E. Svensson *et al.*, Nucl. Instrum. Methods Phys. Res., Sect. B **204**, 660 (2003).
[18] G. C. Ball *et al.*, J. Phys. G **31**, S1491 (2005).

[19] P. E. Garrett *et al.*, Nucl. Instrum. Methods Phys. Res., Sect. B **261**, 1084 (2007).
[20] S. Baker and R. D. Cousins, Nucl. Instrum. Methods Phys. Res., Sect. A **221**, 437 (1984).
[21] S. Agostinelli *et al.*, Nucl. Instrum. Methods Phys. Res., Sect. A **506**, 250 (2003).
[22] Z. Kis *et al.*, Nucl. Instrum. Methods Phys. Res., Sect. A **418**, 374 (1998).
[23] D. C. Radford, RADWARE software package, [http://radware.phy.ornl.gov/].
[24] G. F. Grinyer *et al.*, Nucl. Instrum. Methods Phys. Res., Sect. A **579**, 1005 (2007).